Electric Power Systems Research 140 (2016) 708–721

Contents lists available at ScienceDirect

Electric Power Systems Research

journal homepage: www.elsevier.com/locate/epsr

Coordinated tuning of the parameters of PI, PSS and POD controllers using a Specialized Chu–Beasley's Genetic Algorithm

Elenilson de Vargas Fortes[a,*], Percival Bueno de Araujo[b], Leonardo H. Macedo[b]

[a] Instituto Federal de Goiás, Rua Maria Vieira Cunha 775, Residencial Flamboyant, 75804-714 Jataí, GO, Brazil
[b] Universidade Estadual Paulista, Av. Brasil 56, Centro, PO Box 31, 15385-000 Ilha Solteira, SP, Brazil

ARTICLE INFO

Article history:
Received 2 February 2016
Received in revised form 19 April 2016
Accepted 20 April 2016
Available online 16 June 2016

Keywords:
Current sensitivity model
Interline power flow controller
Power system stabilizers
Power oscillation damping
Specialized Chu–Beasley's Genetic Algorithm

ABSTRACT

This paper presents a Specialized Chu–Beasley's Genetic Algorithm (SCBGA) to perform coordinated tuning of the parameters of proportional-integral and supplementary damping controllers (power system stabilizers and interline power flow controller-power oscillation damping) in multi-machine electric power systems. The objective is to insert additional damping to low frequency electromechanical oscillations. The current sensitivity model was used to represent the system, therefore all of its devices and components were modeled by current injection. A novel current injection model for the interline power flow controller is presented and a static analysis is considered to validate it. The New England test system – consisting of 10 generators, 39 buses, and 46 transmission lines, divided into two areas with both local and inter-area oscillation modes – was used for the simulations. The SCBGA was compared to other five algorithms: a Random Search, a Local Search, a Simulated Annealing, a Genetic Algorithm, and a Particle Swarm Optimization method, in terms of performance for the tuning of the parameters of the controllers. The results demonstrated that the SCBGA was more efficient than these other techniques. In addition, the obtained solutions proved to be robust when variation of the loads was considered.

© 2016 Elsevier B.V. All rights reserved.

1. Introduction

Today's electric power systems (EPSs) are characterized by their diversity in the generation, transmission, and distribution of energy, making their operation more complex. Basic principles such as keeping adequate voltage and frequency levels within the EPS and ensuring the power supply experiences as few interruptions as possible, guarantees the stability of the EPS and so its safety and reliability to energy consumers.

Stability is defined as the ability of an EPS to remain in equilibrium under normal operating conditions; when subjected to disturbances, which can be of small or large magnitude [1], EPSs should evolve to a new operating condition that satisfies the basic principles of generation, transmission and distribution of electrical power. The study of normal load variation at the buses of the EPS is called small signal stability [1].

The small disturbances in EPSs result from low frequency electromechanical oscillations that are classified as: local (0.8–2.0 Hz), inter-area (0.2–0.7 Hz), or intraplant (1.5–2.5 Hz). The type of oscillation is identified by analyzing the frequency of their occurrence [1–3]. The presence of these oscillations in an EPS can affect its operation and even make it unstable; for this reason, strategies to introduce additional damping to the EPS should be applied.

The first studies on electromechanical oscillations were presented by [2] and subsequently by [3]. These studies used supplementary power system stabilizers (PSS) for providing additional damping to oscillations of a synchronous machine rotor. When the parameters of the PSS (time constants and gains) are well adjusted, additional damping is introduced to local mode oscillations [2,3]. However, PSSs are not efficient to provide additional damping to inter-area mode oscillations. On the contrary, depending on the adjustments the effect may be the opposite of what is desired, thereby contributing to the instability of the EPS [4].

Flexible AC transmission systems (FACTS) [5] devices are based on power electronics and are mainly used to control both active and reactive power flows at certain locations of an electric power transmission system. They may also improve voltage levels of EPSs near to their installation. Studies show that if power oscillation damping (POD) controllers are installed in the control loop of FACTS

* Corresponding author.
E-mail addresses: elenilson.fortes@ifg.edu.br (E. de Vargas Fortes), percival@dee.feis.unesp.br (P.B. de Araujo), leohfmp@gmail.com (L.H. Macedo).

http://dx.doi.org/10.1016/j.epsr.2016.04.019
0378-7796/© 2016 Elsevier B.V. All rights reserved.

controllers [6], it is possible that the FACTS-POD pair introduces additional damping to inter-area mode oscillations [7,8].

This paper analyzes the performance of the IPFC FACTS device [9] in the control of active and reactive power flows on the transmission lines of its installation, to correct possible problems of low voltage in the EPS. Furthermore, it will evaluate the influence of the IPFC on small signal stability of the EPS. In [10], the IPFC's inclusion in the Newton–Raphson power flow solution is modeled and in [11], the authors use the IPFC modeled by power injection in the analysis of small signal stability being performed with an EPS represented by the power sensitivity model (PSM) [12]. Additionally in [13], the authors propose a current injection model for the IPFC and have considered a shunt current source for the deduction of the model, with the goal being to improve the EPS's dynamic stability. Finally, in [14] the current injection model for the IPFC is based on the Newton–Raphson method (similar to the model proposed in [11]). In this work, the currents injected by the IPFC are obtained after the convergence of the "expanded current flow". A comparison with other methods based on expanded flows is also made. The structure of the IPFC control system used in the management of active and reactive power flows is based on the proportional-integral (PI) controller, which in turn is based on the works shown in [8,15].

After determining the installation locations of the IPFC and supplementary damping controllers, it is necessary to make correct adjustments of their parameters to provide adequate damping to the EPS. Methods based on classic control techniques such as residues [16], Nyquist's stability criterion [17], and decentralized modal control (DMC) [8,18] have been used successfully in tuning the PSS and POD parameters, but without considering the presence of the IPFC in the system. Recently, optimization methods such as the Bacterial Foraging Optimization Algorithm [19,7], Particle Swarm Optimization [20,21], and Genetic Algorithm (GA) [22] have joined the list of possible techniques used to adjust the parameters of these controllers, considering the operation of the following FACTS devices: thyristor controlled series compensator (TCSC), static var compensator (SVC), and unified power flow controller (UPFC).

One of the contributions of this work is the proposal to perform simultaneous tuning of the parameters of the PI and supplementary damping controllers (PSS and POD) using an optimization technique based on a GA [23] called the Chu–Beasley's Genetic Algorithm (CBGA) [24]. The CBGA has been specially modified to meet the demands of the problem considered in this paper; this adaptation will be called the Specialized Chu–Beasley's Genetic Algorithm (SCBGA).

To analyze the efficiency of the proposed SCBGA for adjusting the parameters of the PI, PSS, and POD controllers to introduce damping to the EPS, the SCBGA's performance is compared to five other algorithms presented in the literature: a Random Search (RS), a Local Search (LS), a Simulated Annealing (SA), a GA [25], and a PSO method [26].

Because of the characteristics of the problem addressed in this work, the variables of each individual in the GA's population are continuous and not binary as proposed in classical GA [25]. This evolutionary proposal is presented in [27]. The PSO algorithm was originally proposed to solve unconstrained continuous optimization problems and in this paper, it was adapted to solve a constrained problem.

From the above, the main contributions of this work are: (1) to present a current injection model for the IPFC; (2) to implement computationally dynamic models of the PSS and the IPFC-POD pair in the current sensitivity model (CSM) for multi-machine systems; and (3) to present and computationally implement the SCBGA to investigate its efficiency to tune the parameters of the PI, PSS, and the IPFC-POD controllers.

2. Current sensitivity model

The CSM is a linear analysis tool for EPSs. Its fundamental concept is based on the application of Kirchhoff's current law; algebraic equations are obtained for the CSM by balancing the currents at all buses, which must be satisfied for all dynamic processes in the EPS [28]. Balanced conditions without saturation are assumed in the deduction of the CSM with the synchronous generator being represented by three stator windings and one rotor winding.

In a multi-machine system represented by the CSM, the state variables (Δx) are: the angular velocity of the rotor in a synchronous machine ($\Delta\omega$), the internal angle of the generator rotor ($\Delta\delta$), the quadrature-axis component of the internal voltage ($\Delta E'_q$), and the field voltage of the generator (ΔE_{fd}). The input variables (Δu) are: the input mechanical power (ΔP_m), the reference voltage (ΔV_{ref}) of the automatic voltage regulator (AVR) of each generator, and the variations of the active (ΔP_l) and reactive (ΔQ_l) loads. Algebraic variables (Δz) are represented by the magnitude (ΔV) and phase angle ($\Delta\theta$) of the voltage of each EPS bus.

The representation in the time domain of a multi-machine EPS – composed of *ng* generators and *nb* buses – modeled by the CSM is given by (1)–(4). More detailed information about (1)–(4) can be found in [28].

$$[\Delta x]=[[\Delta\omega_1\cdots\Delta\omega_{n_g}][\Delta\delta_1\cdots\Delta\delta_{n_g}][\Delta E'^1_q\cdots\Delta E'^{n_g}_q][\Delta E^1_{fd}\cdots\Delta E^{n_g}_{fd}]]^t \tag{1}$$

$$[\Delta u]=[[\Delta P^1_m\cdots\Delta P^{n_g}_m][\Delta V^1_{ref}\cdots\Delta V^{n_g}_{ref}][\Delta P^1_l\cdots\Delta P^{n_b}_l][\Delta Q^1_l\cdots\Delta Q^{n_b}_l]]^t \tag{2}$$

$$[\Delta z]=[[\Delta\theta_1\cdots\Delta\theta_{n_b}][\Delta V_1\cdots\Delta V_{n_b}]]^t \tag{3}$$

$$\begin{bmatrix}\Delta\dot{x}\\0\end{bmatrix}=\begin{bmatrix}J1 & J2\\ J3 & J4\end{bmatrix}\begin{bmatrix}\Delta x\\ \Delta z\end{bmatrix}+\begin{bmatrix}B1\\ B2\end{bmatrix}\begin{bmatrix}\Delta u\end{bmatrix} \tag{4}$$

3. Interline power flow controller device

The IPFC is a fourth generation FACTS device that was first proposed in [9]. This device makes use of voltage source converter technology (VSC) and combines two or more synchronous static series compensators (SSSCs) coupled via a common DC link. The parameters defining the power flow on transmission lines (control of the voltage and the angles at the EPS buses, for example) can be controlled simultaneously – or selectively – using this combination. This implies that, depending on the adopted configuration, the flow of active and reactive power can be controlled and series compensation can be achieved on the transmission lines where the IPFC is installed. Fig. 1 shows a model of the equivalent circuit of the IPFC.

In Fig. 1, P_i and Q_i are the injections of active and reactive power at bus *i*. P_{ji} and Q_{ji} are the flows of active and reactive power (leaving bus *j*) of the common installation branch of the IPFC. Similarly, P_{ki} and Q_{ki} indicate the flows of active and reactive power leaving bus *k* (common to the IPFC installation). Moreover, $\mathbf{I}_{ij}$ and $\mathbf{I}_{ik}$ designate the currents that leave bus *i*, while $\mathbf{I}_{ji}$ and $\mathbf{I}_{ki}$ represent the currents leaving buses *j* and *k*, respectively.

Assuming that the active losses are zero, the active power provided by one of the converters will always be equal to the active

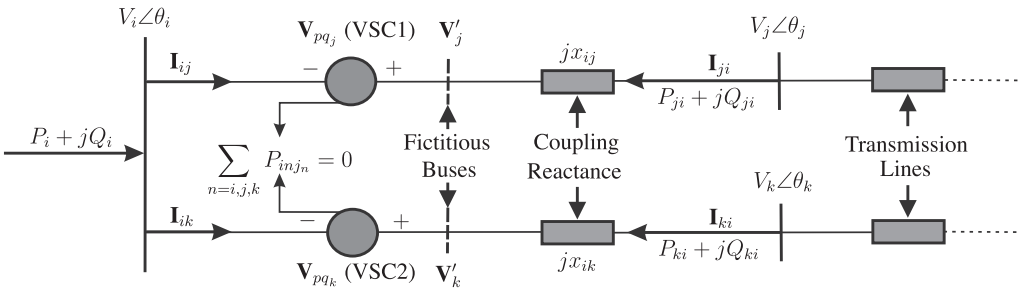

Fig. 1. Equivalent circuit of an IPFC with two series voltage sources.

power demanded by the other, as shown in (5). This restriction is also known as the active power invariance of the IPFC [10].

$$\sum_{n=i,j,k} P_{inj_n} = 0 \tag{5}$$

The control of power flow on the transmission line in which the IPFC is installed is accomplished by controlling the magnitude and angle of the series voltages $\mathbf{V}_{pq_n}$ ($n=j,k$) as represented in (6) (see Fig. 2).

$$\mathbf{V}_{pq_n} = r_n e^{j\gamma_n}\mathbf{V}_i \tag{6}$$

In Fig. 2, the variables γ_n ($0<\gamma_n<2\pi$) and r_n ($0<r_n<r_n^{\max}$) are the parameters of the series voltages ($\mathbf{V}_{pq_n}$), $r_n=\frac{\mathbf{V}_{pq_n}}{\mathbf{V}_i}$ and γ_n is the angle of $\mathbf{V}_{pq_n}$ with respect to the voltage of bus i ($\mathbf{V}_i$) [29]. V_{qn} and V_{pn}, represent the components in phase and in quadrature of the controllable series voltage, as shown in (7) and (8), respectively.

$$\mathbf{V}_{qn} = r_n\mathbf{V}_i\cos\gamma_n \tag{7}$$

$$\mathbf{V}_{pn} = r_n\mathbf{V}_i\sin\gamma_n \tag{8}$$

Details of the IPFC power injection model can be found in [8,29].

3.1. Current injection model for the IPFC

Differing from the proposal in [14,30], in this work the IPFC will be modeled based on the equivalent circuit shown in Fig. 1. The currents injected by the device will be calculated directly from the series voltage sources (considering the reactances of the respective coupling transformers in respect of each series voltage source). Furthermore, the proposed current injection model has a significant advantage as it is independent of the parameters r_n and γ_n of (6), thereby eliminating the need to calculate these variables (steps not performed in [14,30]).

By inspecting the equivalent circuit shown in Fig. 1, (9) and (10) are obtained.

$$\mathbf{I}_i = \mathbf{I}_{ij}+\mathbf{I}_{ik} = \left(\frac{V_i\angle\theta_i + r_j e^{j\gamma_j}V_i - V_j\angle\theta_j}{jx_{ij}}\right) + \left(\frac{V_i\angle\theta_i + r_k e^{j\gamma_k}V_i - V_k\angle\theta_k}{jx_{ik}}\right) \tag{9}$$

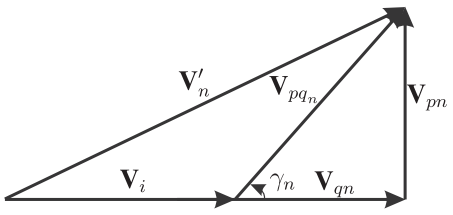

Fig. 2. Phasor diagram of the IPFC ($n=j,k$).

$$\mathbf{I}_{ni} = \frac{(V_n - V'_n)}{jx_{in}} = \left(\frac{V_n\angle\theta_n - V_i\angle\theta_i - r_n e^{j\gamma_n}V_i\angle\theta_i}{jx_{in}}\right) \tag{10}$$

Eqs. (11)–(14) are determined after considering (5), (7)–(10), where $b_{in}=-\frac{1}{x_{in}}$ for $n=j,k$.

$$I_{i_r} = -V_i\sin\theta_i(b_{ij}+b_{ik}) + b_{ij}V_j\cos\theta_j + b_{ik}V_k\sin\theta_k \underbrace{-\sum_{n=j,k} b_{in}(V_{pn}\cos\theta_i + V_{qn}\sin\theta_i)}_{\text{IPFC}} \tag{11}$$

$$I_{i_m} = V_i\cos\theta_i(b_{ij}+b_{ik}) - \sum_{n=j,k} b_{in}V_n\cos\theta_n \underbrace{+\sum_{n=j,k} b_{in}(V_{qn}\cos\theta_i - V_{pn}\sin\theta_i)}_{\text{IPFC}} \tag{12}$$

$$I_{ni_r} = b_{in}(V_i\sin\theta_i - V_n\sin\theta_n) + \underbrace{b_{in}(V_{pn}\cos\theta_i + V_{qn}\sin\theta_i)}_{\text{IPFC}} \tag{13}$$

$$I_{ni_m} = b_{in}(V_n\cos\theta_n - V_i\cos\theta_i) + \underbrace{b_{in}(V_{pn}\sin\theta_i - V_{qn}\cos\theta_i)}_{\text{IPFC}} \tag{14}$$

The current injection model of the IPFC FACTS is obtained after the analysis of (11)–(14). The underlined parts with the label "IPFC" are the contributions of the device to the current flow in common installation buses. $I_{inj_{i_r}}$ and $I_{inj_{i_m}}$ are injected at bus i, while the currents $I_{inj_{n_r}}$ and $I_{inj_{n_m}}$, the real and imaginary components, are injected at buses n ($n=j,k$), as shown in Fig. 3.

3.2. Structure of the IPFC control system

The control of the active and reactive power flows by the IPFC is performed by PI controllers (see Fig. 4).

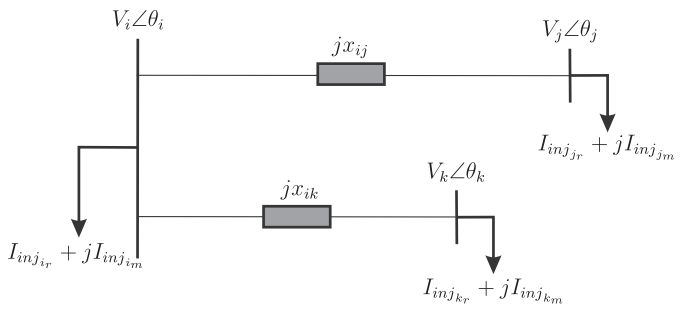

Fig. 3. Current injection model for the IPFC.

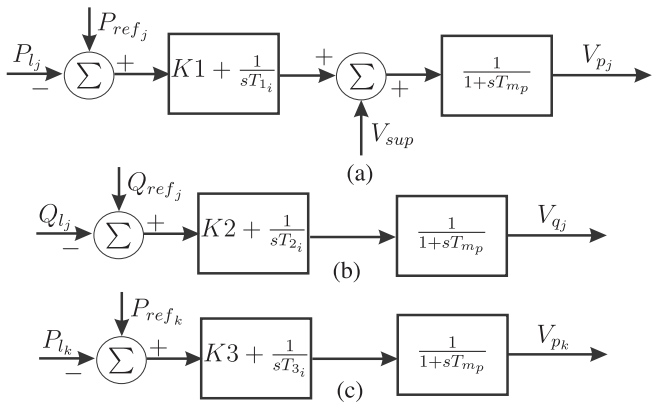

Fig. 4. Structure of the IPFC control system.

These PI controllers are related to the variables of the controllable sources V_{p_j}, V_{p_k}, and V_{q_j}. The variable V_{q_k} is associated with the equation of active power invariance (5). In the structure presented, the time constant, T_{m_p} is the delay inherent to the control device with values stipulated between 1 and 10 ms [5]. Furthermore, the parameters of the controllers are indicated by the gains $K1$, $K2$, and $K3$ (in p.u.) and the time constants T_{1_i}, T_{2_i}, and T_{3_i} (in seconds). The supplementary signal V_{sup} (Fig. 4(a)) results from the POD controller and in this article it is used to modulate the quadrature component (V_{p_j}) of the first converter (VSC1).

In the management of the active and reactive power flows shown in Fig. 4, the controlled powers (P_{l_j}, P_{l_k}, and Q_{l_j}) and reference powers (P_{ref_j}, Q_{ref_j}, and Q_{ref_k}) obey the control laws shown in (15)–(17).

$$P_{l_j} - P_{ref_j} = 0 \tag{15}$$

$$P_{l_k} - P_{ref_k} = 0 \tag{16}$$

$$Q_{l_j} - Q_{ref_j} = 0 \tag{17}$$

The differential equations that represent the dynamics of the control system of the PI controllers are given by (18)–(23) and are obtained by analyzing Fig. 4.

$$\dot{V}_{p_j} = \frac{K_1}{T_{m_p}}(P_{ref_j} - P_{l_j}) + \frac{1}{T_{m_p}}(X_1 + V_{\text{sup}} - V_{p_j}) \tag{18}$$

$$\dot{X}_1 = \frac{1}{T_{1_i}}(P_{ref_j} - P_{l_j}) \tag{19}$$

$$\dot{V}_{q_j} = \frac{K_2}{T_{m_p}}(Q_{ref_j} - Q_{l_j}) + \frac{1}{T_{m_p}}(X_2 - V_{q_j}) \tag{20}$$

$$\dot{X}_2 = \frac{1}{T_{2_i}}(Q_{ref_j} - Q_{l_j}) \tag{21}$$

$$\dot{V}_{p_k} = \frac{K_3}{T_{m_p}}(P_{ref_k} - P_{l_k}) + \frac{1}{T_{m_p}}(X_3 - V_{p_k}) \tag{22}$$

$$\dot{X}_3 = \frac{1}{T_{3_i}}(P_{ref_k} - P_{l_k}) \tag{23}$$

4. Structure of the PSS and POD controllers

The inclusion of supplementary damping controllers (PSS and POD) in the EPS is necessary to introduce additional damping to low frequency electromechanical oscillations. Fig. 5 shows the structure that will be used for the PSS and POD controllers. The structures are identical; differing only in the input and output signals of the two controllers. In the case of the PSS, the input signal (ΔV_{in}) is represented by the variations of the deviations in angular velocity ($\Delta\omega_k$) of the rotor of generator k, and in the POD it is the deviations in active power of the transmission line adjacent to the installation of the device (ΔP_{km}). The output of the PSS (ΔV_{sup_1}) is applied to the control loop of the voltage generator and the output of the POD (ΔV_{sup_2}) is added to the control loop of the IPFC (Fig. 5).

In Fig. 6(a), the AVR is represented by a gain, K_{r_k} and a time constant, T_{r_k}. The excitation voltage of the synchronous machine is E_{fd_k}, the variation in terminal voltage of the generator k is ΔV_k and the variation of the reference voltage is V_{ref_k}. In Fig. 6(b), ΔV_{p_j} is the quadrature-axis component of the primary converter (VSC1) related to the installation of the POD, ΔX_{ref} is an input signal and T_{m_p} is a time constant, both of which must be specified.

Eqs. (24)–(27) which represent the dynamic behavior of the PSS and (28)–(31) which represent the dynamic behavior of the POD controller, are obtained by analyzing Figs. 5 and 6.

$$\Delta\dot{V}_{1_k} = \Delta\dot{\omega}_k K_{pss} - \frac{1}{T_\omega}\Delta V_{1_k} \tag{24}$$

$$\Delta\dot{V}_{2_k} = \frac{1}{T_2}\Delta V_{1_k} + \frac{T_1}{T_2}\Delta\dot{V}_{1_k} - \frac{1}{T_2}\Delta V_{2_k} \tag{25}$$

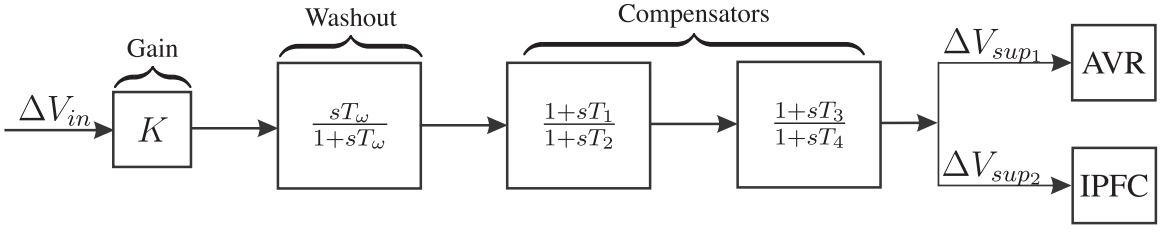

Fig. 5. Dynamic model of the PSS and POD controller.

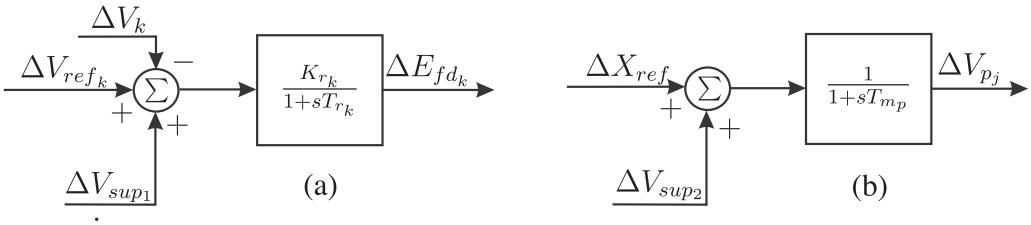

Fig. 6. Dynamic model of the PSSs and POD: (a) Control loop of the AVRs; (b) Quadrature voltage component of the primary converter of the IPFC.

$$\Delta\dot{V}_{sup_1} = \frac{1}{T_4}\Delta V_{2_k} + \frac{T_3}{T_4}\Delta\dot{V}_{2_k} - \frac{1}{T_4}\Delta V_{sup_1} \tag{26}$$

$$\Delta\dot{E}_{fd_k} = \frac{K_r}{T_r}(\Delta V_{sup_1} + \Delta V_{ref_k} - \Delta V_k) - \frac{1}{T_r}\Delta E_{fd_k} \tag{27}$$

$$\Delta\dot{Y}_1 = \frac{1}{T_{\omega_p}}(K_{pod}\Delta P_{km} - \Delta Y_1) \tag{28}$$

$$\Delta\dot{Y}_2 = \frac{1}{T_{p_2}}\left[\left(1 - \frac{T_{p_1}}{T_{p_2}}\right)(K_{pod}\Delta P_{km} - \Delta Y_1) - \Delta Y_2\right] \tag{29}$$

$$\Delta\dot{Y}_3 = \frac{1}{T_{p_4}}\left\{\left[\Delta Y_2 + \frac{T_{p_1}}{T_{p_2}}(K_{pod}\Delta P_{km} - \Delta Y_1)\right]\left(1 - \frac{T_{p_3}}{T_{p_4}}\right) - \Delta Y_3\right\} \tag{30}$$

$$\Delta\dot{V}_{p_j} = \frac{K_1}{T_{m_p}}(\Delta P_{ref_j} - \Delta P_{l_j}) + \frac{1}{T_{m_p}}(\Delta X_1 + \Delta V_{sup_2} - \Delta V_{p_j}) \tag{31}$$

In (24)–(31) T_1, T_2, T_3, T_4, and K_{pss} are the time constants and gain of the PSS. T_{p_1}, T_{p_2}, T_{p_3}, T_{p_4}, and K_{pod} are the time constants and gain of the POD; it is usual to adopt $T_1(T_{p_1}) = T_3(T_{p_3})$ and $T_2(T_{p_2}) = T_4(T_{p_4})$ [31]. Moreover, ΔV_{sup_2} is defined in (32).

$$\Delta V_{sup_2} = \Delta Y_3 + \frac{T_{p_3}}{T_{p_4}}\left[\Delta Y_2 + \frac{T_{p_1}}{T_{p_2}}(K_{pod}\Delta P_{km} - \Delta Y_1)\right] \tag{32}$$

5. Technique to tune the parameters of the PI, PSS, and POD controllers

Based on the modeling of the EPS and the dynamic models of the PI, PSS, and IPFC-POD controllers, this section will present a specialized evolutionary algorithm based on the proposal of Chu and Beasley [24].

5.1. Specialized Chu–Beasley's Genetic Algorithm (SCBGA)

The proposal by Chu and Beasley [24] for the GA includes the representation of a solution proposal for each specific type of problem, separate fitness and unfitness evaluations, and a local improvement procedure. In addition, they proposed an analysis to replace an individual in a population. The following changes to the CBGA, with their justifications are suggested for this work:

1. *Implement a step to improve the initial population:* it was found experimentally that the application of a local search algorithm to members of the initial population reduces the computational effort needed to solve the problem;
2. *Use a small population:* the problem is characterized by the presence of continuous variables. In this case, the local improvement step may require great computational effort to improve the initial population. Therefore, a small initial population is recommended;
3. *Variation operator:* the proposal is to make a combination of solutions, element by element, in which each component of the first descendant is obtained as the sum of the components of two generating solutions, each one multiplied by two random weighting factor β (for the first parent) and $(1-\beta)$ (for the second parent), where $0 \le \beta \le 1$. The second descendant is obtained from multiplying the first parent by $(1-\beta)$ and the second by β;
4. *Maintaining the descendant with the best fitness value:* in the original proposal by Chu and Beasley, the choice of a descendant to be improved is random. The purpose of this study is to improve the descendant with the best (lowest) fitness value. It is hoped that this is the most promising way to find better quality solutions;
5. *Eliminate the mutation step:* the mutation is used in the traditional GA so that characteristics that are not present in the population may appear. However, the local improvement step eliminates this need.

Fig. 7 shows the operational structure of the Specialized Chu–Beasley's Genetic Algorithm.

5.2. Local search

The local search strategy consists of discretizing the search space and carrying out changes to the variables of the problem.

Assume that the solution x^r is preserved after the application of the variation operator. Then define the evaluation function of x^r, $F(x^r)$, as shown in (33).

$$F(x^r) = f(x^r) + \rho h(x^r) \tag{33}$$

$$f(x^r) = \sum_{i=1}^{n} |\lambda_i^{calc} - \lambda_i^{des}| \tag{34}$$

$$h(x^r) = \sum_{i=1}^{n} |\xi_i^{calc} - \xi_i^{des}| \tag{35}$$

In (33), the evaluation function $F(x^r)$ is composed of the objective function $f(x^r)$ summed to an infeasibility $h(x^r)$ ($\rho \gg 1$ is a penalty parameter). In (34) and (35), n indicates the number of eigenvalues of interest of the EPS, with λ_i^{calc} being the calculated eigenvalues of interest, λ_i^{des} the desired eigenvalues of interest, ξ_i^{des} the desired

Algorithm 1: **Specialized Chu-Beasley's Genetic Algorithm**

1 **Initialization**: Specify control parameters: the initial population size, recombination rate, determine general characteristics of the algorithm: encoding type, the initial population size, manipulation of infeasibilities;
2 Randomly find an initial population, which becomes the current population. Find the fitness and unfitness of the members of the current population;
3 Apply the **local improvement** step to the initial population;
4 **Repeat** steps (5) to (8) until the stop criterion is satisfied:
5 Implement the selection by tournament to pick just two generating solutions;
6 Implement the variation operator and preserve the descendant with the lowest fitness value;
7 Implement a **local improvement phase**;
8 Decide whether the improved descendant enters the current population;

Fig. 7. Operating structure of the SCBGA.

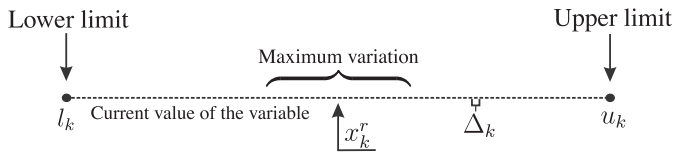

Fig. 8. Discretization of a variable in the local improvement step.

damping, and ξ_i^{calc} the calculated damping at each iteration performed by the local search.

A vector of sensitivities, $\mathbf{s} = [s_1, s_2, \ldots, s_{n_v}]$ is defined, where n_v is the number of variables in the problem. Initially $s_i = 0$, $\forall i = 1, \ldots, n_v$. The value of each discretization step for variable i, Δ_i, is determined as shown in (36), where u_i and l_i are, respectively, the upper and lower limits of the variable x_i^r, and Γ is the whole number of discretizations.

$$\Delta_i = \frac{u_i - l_i}{\Gamma}, \quad i = 1, \ldots, n_v \tag{36}$$

A variable of the problem is chosen at random to modify its value. Suppose the variable x_k^r is chosen. Fig. 8 shows how x_k^r is discretized.

The value of the variation δ_k is shown in (37), where φ is a random number ($0 \le \varphi \le 1$), γ is a scaling factor, and $\lceil . \rceil$ is the ceiling function, which rounds the value ($\gamma\varphi$) up to the next whole number.

$$\delta_k = \lceil \gamma\varphi \rceil \Delta_k \tag{37}$$

Then, the new value of x_k^r is determined by (38).

$$\widetilde{x}_k^r = x_k^r \pm \delta_k \tag{38}$$

In (38), as originally $s_k = 0$, an increase or decrease of the value of the variable x_k^r is chosen with equal probability. Note that in (38), $\widetilde{x}_k^r$ may violate the lower l_k or upper u_k bounds. In this case, consider the correction shown in (39).

$$\hat{x}_k^r = \begin{cases} \widetilde{x}_k^r, & \text{if } \; l_k \le \widetilde{x}_k^r \le u_k \\ l_k, & \text{if } \; \widetilde{x}_k^r < l_k \\ u_k, & \text{if } \; \widetilde{x}_k^r > u_k \end{cases} \tag{39}$$

Finally, the solution must be updated; designate the new solution obtained as $\hat{x}^r$. The evaluation function, $F(\hat{x}^r)$ is then calculated to check the quality of the new solution proposal. Two situations can then occur:

1. $F(\hat{x}^r) < F(x^r)$: in this case, s_k is defined as 1 if in (38) x_k^r was incremented or s_k is designated -1 if in (38) x_k^r was decremented. Furthermore, the current solution is updated $x^r \longleftarrow \hat{x}^r$;
2. $F(\hat{x}^r) \ge F(x^r)$: in this case, s_k is defined as -1 if in (38) x_k^r was incremented or s_k is defined as 1 if in (38) x_k^r was decremented; here the current solution is not updated.

The described procedure is then repeated, i.e., another variable is chosen to have its value changed. In (38) however, one must consider the value of s_k, i.e., if $l_k \le x_k^r \le u_k$ and $s_k = 1$, then the value of x_k^r must be incremented; if $s_k = -1$ the value x_k^r must be decremented; if $s_k = 0$, randomly choose between incrementing or decrementing x_k^r.

Now, for situations in which $x_k^r = l_k$ or $x_k^r = u_k$, x_k^r must be incremented (if $x_k^r = l_k$) or decremented (if $x_k^r = u_k$) regardless of the value of s_k.

This process is repeated until no further improvement is obtained or until a maximum number of iterations, Υ, have been performed without improvement. The factor γ should be adjusted dynamically during the process; that is, from τ iterations, $\tau < \Upsilon$, without improvement of the evaluation function, update $\gamma \longleftarrow \frac{\gamma}{2}$ in (37).

The local improvement is applied both to the initial population and to individuals recombined in the local search. The following values were adopted in this work: $\rho = 10^3$, $\Gamma = 100$, and $\gamma = 20$. Fig. 9 shows the algorithm of the local search methodology.

5.3. Overview for the optimization problem

Consider an EPS equipped with n PSS controllers in n synchronous machines and an IPFC-POD. To determine the gains and time constants of the controllers shown in Figs. 4 and 5, a solution proposal is presented for an individual belonging to the population of the SCBGA (Fig. 10).

Note that the first n positions of the individual represented in Fig. 10 are destined to the n time constants T_{1_i} of n PSS controllers installed in n synchronous generators. The position $n+1$ refers to the time constant T_{p_1} of the IPFC-POD. Continuing in order, the n time constants T_{2_i} and then T_{p_2}, the n gains K_{pss} ($K_1, \ldots, K_n$) and the gain K_{pod} (K) are represented. The last positions of the individual are reserved for the parameters of the PI controllers (T_{i_j} and K_j, where $j = 1, 2, 3$).

Each individual belonging to the initial population or the population improved by the SCBGA (Fig. 10) is subject to the restrictions imposed in (40)–(42) (time constants in seconds and gains in p.u.).

$$0.1 \le T_{1_n} \le 1.5; \quad 0.01 \le T_{2_n} \le 0.1; \quad 1.0 \le K_{pss} \le 10.0 \tag{40}$$

$$0.1 \le T_{p_1} \le 0.4; \quad 0.1 \le T_{p_2} \le 0.4; \quad 1.0 \le K_{pod} \le 0.4 \tag{41}$$

$$0.001 \le T_{i_j} \le 0.01; \quad 0.1 \le K_j \le 1.5 \tag{42}$$

Values for the limits (40)–(42) are found in [19–22], differing from one another. In this paper, the upper bounds for the gains of the controllers are lower than the ones found in the cited literature, since high gains for the controllers indicate greater control effort and in some cases, it may be impractical. As it will be observed in Section 6, it is possible to provide high levels of damping to the modes of interest with the settings provided by the SBGA with low gains and time constants in the considered range of values.

The goal of the proposed approach is to solve a constraint satisfaction problem [25]. In this case, the desired damping is considered a constraint, and thus any adjustment that provides the desired damping is considered a solution.

The objective function used to obtain the desired damping for a solution proposal is defined in (34) and consists of minimizing the distance between the calculated eigenvalues of interest (λ_i^{calc}) and the desired eigenvalues of interest (λ_i^{des}). Thus, λ_i^{calc} is positioned in a particular region of interest of the complex plane at each iteration after adjusting the parameters of the PI, PSS, and IPFC-POD controllers (using the SCBGA with the appropriate restrictions set forth in (40)–(42)). The desired eigenvalues of interest (λ_i^{des}) are defined by design to satisfy the desired damping coefficient (ξ_i^{des}). The calculated eigenvalues of interest (λ_i^{calc}) are determined at each iteration for the EPS by the CSM. This procedure is shown in Fig. 11.

6. Simulations and results

The solution methods and the modeling presented in the previous sections were implemented in MATLAB, without the aid of any toolbox. Simulations were then performed to analyze small signal stability using the New England system [18]. The tests were carried out on a computer with a 2.60 GHz Intel Core i5-3230M processor and 12 GB of RAM.

In this study, two damping ranges are specified for all the calculated eigenvalues of interest (λ_i^{calc}), greater than a lower limit of $\xi_{i_{\min}}^{des_1} = 10\%$ in the first case, and $\xi_{i_{\min}}^{des_2} = 15\%$ in a second test. These two damping ranges are considered to evaluate the performance of the algorithms analyzed in this paper. The time constant of the

Algorithm 2: Local search

Initialization: Specify the parameters: $\rho, \Gamma, \gamma, \tau, \Upsilon$; Initialize the sensitivity vector, $\mathbf{s}$, with all positions set to zero; Calculate the discretization step of each variable, $\Delta_i \longleftarrow (u_i - l_i)/\Gamma$, $i = 1, \cdots, n_v$; $t \longleftarrow 0$; $m \longleftarrow 0$;
While $t \leq \Upsilon$:
  Randomly choose a variable k that will have its value changed, x_k^r, in the current solution of the local search x^r;
  Calculate the value of the change $\delta_k \longleftarrow \lceil \gamma\varphi \rceil \Delta_k$;
  Calculate the value of $\tilde{x}_k^r$:
  If $l_k \leq x_k^r \leq u_k$:
    If $s_k = 0$: Choose to increment or decrement the value of x_k^r: $\tilde{x}_k^r \longleftarrow x_k^r \pm \delta_k$, with the same probability;
    Else if $s_k = 1$: $\tilde{x}_k^r \longleftarrow x_k^r + \delta_k$;
    Else: $\tilde{x}_k^r \longleftarrow x_k^r - \delta_k$;
  Else if $x_k^r = l_k$: $\tilde{x}_k^r \longleftarrow x_k^r + \delta_k$;
  Else: $\tilde{x}_k^r \longleftarrow x_k^r - \delta_k$;
  Check if the variable $\tilde{x}_k^r$ is within the range $[l_k, u_k]$:
    If $l_k \leq \tilde{x}_k^r \leq u_k$: $\hat{x}_k^r \longleftarrow \tilde{x}_k^r$;
    Else if $\tilde{x}_k^r < l_k$; $\hat{x}_k^r \longleftarrow l_k$;
    Else: $\hat{x}_k^r \longleftarrow u_k$;
  Assemble the new solution $\hat{x}^r$, coping x^r with the value of $\hat{x}_k^r$ in position k
  Calculate the evaluation function of the new solution, $F(\hat{x}^r)$;
  Update the current solution and the position k of the vector $\mathbf{s}$;
  If $F(\hat{x}^r) < F(x^r)$: $x_k^r \longleftarrow \hat{x}_k^r$; $F(x^r) \longleftarrow F(\hat{x}^r)$; $s_k \longleftarrow 1$ if x_k^r was incremented; $s_k \longleftarrow -1$ otherwise; $m \longleftarrow 0$;
  Else: $s_k \longleftarrow -1$ if x_k^r was incremented; $s_k \longleftarrow 1$ otherwise; $m \longleftarrow m + 1$; $t \longleftarrow t + 1$;
If $m > \tau$: $\gamma \longleftarrow \gamma/2$; $m \longleftarrow 0$;

Fig. 9. Algorithm for local search implemented in the SCBGA.

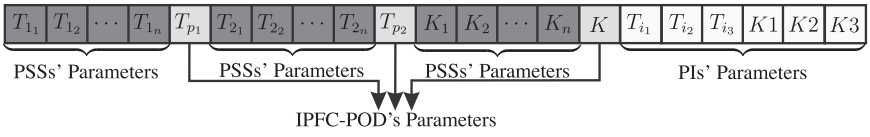

Fig. 10. Representation of an individual in the SCBGA.

washout block (see Fig. 5) was specified to ten seconds for the PSSs (T_ω) and one second for the IPFC-POD (T_{ω_p}). The time constant, T_{m_p} (see Fig. 6) was set to 0.005 s.

6.1. Static analysis for the test system

The New England system comprises 10 generators, 41 buses, and 48 transmission lines; its one line diagram is shown in Fig. 12. Two fictitious buses, FB_1 and FB_2, two lines 37-FB_1 and 37-FB_2, and the reactances of the coupling transformers (x_{in}, $n = j$, k with values stipulated at 0.01 p.u.) are already included in this diagram.

As shown in Fig. 12, the IPFC is installed between buses 37–34 and 37–36. This location was chosen for technical reasons, as it is intended to solve voltage problems at buses 12, 15, 33, 36, and 37, that are less than 0.95 p.u. (see Fig. 13). In this situation, the

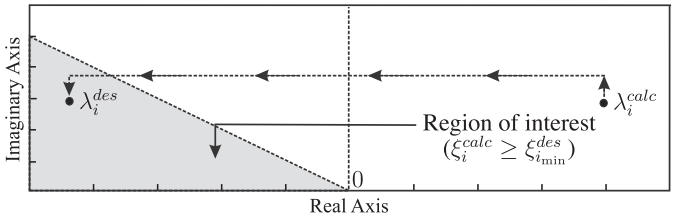

Fig. 11. Location of the desired eigenvalues (λ_i^{des}).

variables of the IPFC are (in p.u.): $V_{p_j} = -8.63 \times 10^{-7}$, $V_{p_k} = -2.47 \times 10^{-6}$, $V_{q_j} = 4.69 \times 10^{-7}$, and $V_{q_k} = -7.52 \times 10^{-7}$. Complete data for this system is presented in Appendix A.

The variables' values of the series converters are close to zero and thus do not exert any control over the active and reactive power flows of the New England system. In this condition, the IPFC is included in the system but without exerting any control on the power flows (Case I).

To solve the problem of existing low voltages in the New England system, the IPFC is required to control flows in the lines FB_1-34 and FB_2-36, making $P_{ref_j} = -410.51$ MW (Case I: −310.98 MW), $Q_{ref_j} = -55.81$ MVAr (Case I: −42.28 MVAr), and $P_{ref_k} = -316,71$ MW (Case I: −241.76 MW). This will be referred to as Case II. These values were chosen conveniently, so that the voltage magnitude at each bus stay within the adequate limits. In this situation, the values of the variables used to represent the converters are (in p.u.): $V_{p_j} = -0.2938$, $V_{p_k} = -0.3049$, $V_{q_j} = -0.0485$, and $V_{q_k} = 0.0048$.

A new voltage profile is found for the New England system when the IPFC exerts control on the active and reactive power flows (see Fig. 13). On analyzing Fig. 13, it is concluded that the IPFC improved the voltage profile of buses 12, 15, 33, 36, and 37, all being within the acceptable range (±5% of the nominal value).

Fig. 14 shows the active power flows in the New England system without any interference from the IPFC (Case I) and with the IPFC (Case II). On analyzing the flows after the inclusion of the IPFC, it is possible to see that the device does not provide active power to

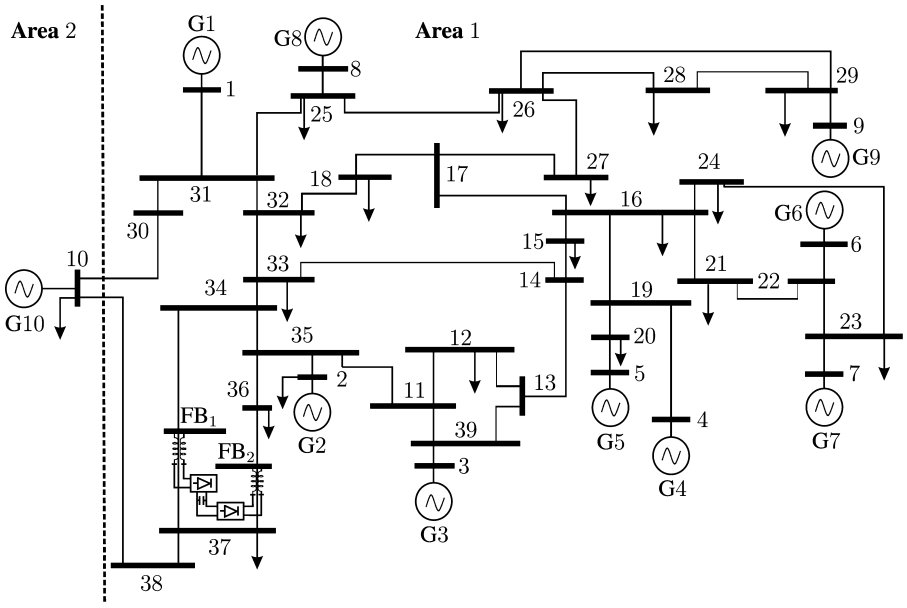

Fig. 12. One-line diagram of the New England system.

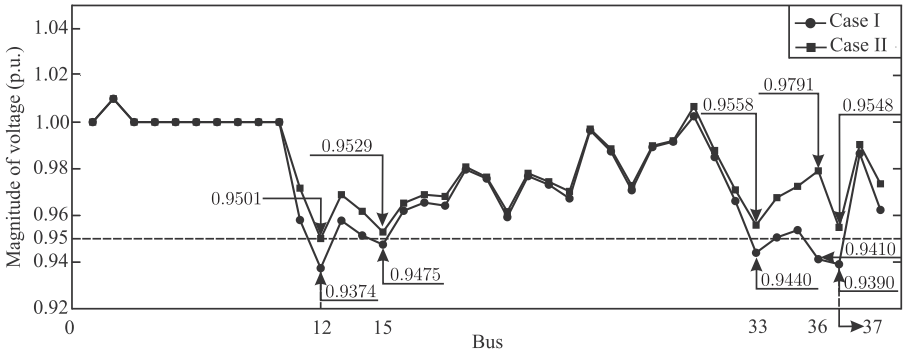

Fig. 13. Profile of the bus voltage magnitudes of the New England system.

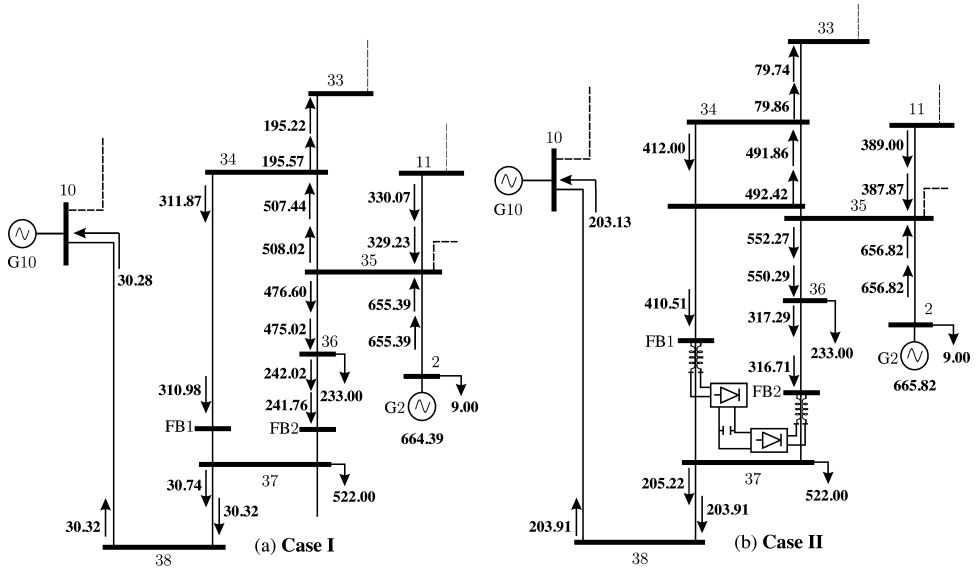

Fig. 14. Control of active power flows performed by the IPFC device.

Table 1
Dominant eigenvalues (λ_i), damping coefficients (ξ_i) and natural undamped frequencies (ω_{ni}) – Case I.

Mode	Eigenvalues	ξ (p.u.)	ω_{ni} (Hz)
λ_1	$0.0484 \pm j6.8621$	−0.0070	1.0922
λ_2	$-0.2198 \pm j7.3085$	0.0301	1.1637
λ_3	$-0.2013 \pm j8.2718$	0.0243	1.3169
λ_4	$0.1508 \pm j5.9600$	−0.0253	0.9489
λ_5	$-0.1351 \pm j6.5134$	0.0184	1.0369
λ_6	$-0.2706 \pm j8.1099$	0.0207	1.2914
λ_7	$-0.2408 \pm j8.3226$	0.0289	1.3251
λ_8	$0.1814 \pm j6.3874$	−0.0284	1.0170
λ_9	$0.0290 \pm j3.8641$	−0.0075	0.6150

the EPS (restriction of active power invariance of the IPFC, (5)), but transfers – or removes – by means of the serial converters, a portion of the active power to the lines where the flows are controlled. With the data shown in Fig. 14, it is possible to balance active power at the buses of the installation of the IPFC and thus validate the flow control achieved by the device.

6.2. Tuning the parameters of the PI controllers and supplementary damping controllers (PSS and IPFC-POD)

Considering the operating conditions in Case II (Section 6.1), the eigenvalues of the New England system are calculated. The oscillation modes of interest ($\lambda_i = \sigma_i \pm j\omega_i$) are shown in Table 1. The undamped natural frequency ($\omega_{ni} = \frac{|\lambda_i|}{2\pi}$) and the damping coefficient ($\xi_i = -\frac{\sigma}{|\lambda_i|}$) associated to each oscillation mode are also shown.

On analyzing the frequencies (ω_{ni}) of the oscillation modes of interest, it is observed that eight are local mode oscillations (λ_1 to λ_8) and only one is an inter-area mode oscillation (λ_9). Of these, four (λ_1, λ_4, λ_8, and λ_9) have positive real parts, showing that the system is unstable at this operating point.

The flow control achieved by the IPFC (Case II) corrected the voltage magnitudes at buses 12, 15, 33, 36, and 37 but it was not enough to insert damping to the oscillation modes of interest (see Table 1). To achieve this, it is recommended to equip the New England system with PSSs and an IPFC-POD, located as shown in Fig. 12.

The locations of the generators that should be equipped with PSSs were identified using the contribution factors [31]. Simulations indicated that the best locations were generators G1, G2, G3, G4, G5, G7, G8, and G9.

6.2.1. Characteristics of the algorithms

The SCBGA was compared with five other algorithms in terms of performance for tuning the parameters of the controllers. The algorithms used for comparison were: a Random Search, a Local Search, a Simulated Annealing, a Genetic Algorithm, and a Particle Swarm Optimization method.

The RS generates random solutions for the problem, one after another, with no additional search strategy. The objective of using this algorithm is to verify if a completely random search would be able to satisfactorily solve the problem for all damping ranges.

The LS strategy shown in Fig. 9 was used to try to solve the problem directly. The search was performed considering five solution proposals in parallel, i.e., it was started from five random points. The parameters of the algorithm were discussed in Section 5.2.

The SA algorithm considered in this paper is an extension of the LS strategy shown in Fig. 9. On line 19 of the algorithm of Fig. 9, it is also assumed that the solution can be updated ($x_k^r \longleftarrow \hat{x}_k^r$) even when $F(\hat{x}^r) \geq F(x^r)$, if a probabilistic criterion is met. If $F(\hat{x}^r) \geq F(x^r)$ and $\exp(\frac{F(x^r)-F(\hat{x}^r)}{T_k}) > P(0,1)$, then $x_k^r \longleftarrow \hat{x}_k^r$, where T_k is the temperature at level N_k and $P(0,1)$ is a random number in the interval [0, 1]. Also, the temperature T_k and the temperature level N_k must be updated after N_k iterations: $T_{k+1} = \mu T_k$ and $N_{k+1} = \eta N_k$. In the implementation, $T_o = 100$, $N_o = 50$, $\mu = 0.7$, and $\eta = 0.9$.

A traditional GA was also implemented: considering a population of 20 individuals, fixed mutation rate of 10%, and tournament selection. This algorithm does not consider the LS strategy shown in Fig. 9.

The PSO method considered uses a population of 20 particles. The acceleration constants are $c_1 = c_2 = 2.05$, and the inertia weight $w \in [0.5, 1.5]$. Additional information about the algorithms presented in this section can be found in [25,26].

For the SCBGA presented in Section 5.1, the population consisted of five individuals, and the LS algorithm was used with the parameters described in Section 5.2.

6.2.2. Performance evaluation of the SCBGA

In this subsection, a comparison of the performance of the six optimization methods is presented. As already stated above, the objective is to perform the coordinated tuning of the parameters of PI, PSS, and POD controllers and thus introduce the desired damping to the test system. The simulations were performed considering two different scenarios: in the first one, to introduce at least 10% of damping to all oscillatory modes ($\xi_{i_{\min}}^{des_1} = 10\%$) and in the second one, to introduce at least 15% of damping to all oscillatory modes ($\xi_{i_{\min}}^{des_2} = 15\%$).

For each of the algorithms 100 tests were performed; each test was limited to a maximum of 2000 objective function evaluations for each algorithm. For all the results of the simulations shown in Table 2 it was considered that the parameters of the controllers must satisfy constraints (40)–(42).

Table 2 shows the number of times that a feasible result was achieved for each group of ten trials. In addition, the convergence times shown in Table 2 refers to the average, minimum, and maximum times in trials for which the algorithms converged, therefore excluding the time spent in attempts when the algorithms did not converge.

The analysis of the data presented in Table 2 can be separated in to cases: for the first case, $\xi_{i_{\min}}^{des_1} \geq 10\%$, the LS, SA, GA, and SBGA converged for 100% of the trials, with average times of 34.60, 89.55, 60.90, and 14.53 s, respectively. The PSO converged for 99% of the trials with an average time of 34.34 s. The RS converged in 11% of the trials with an average time of 212.72 s for the ones in which it converged. In the second case, $\xi_{i_{\min}}^{des_2} \geq 15\%$, the RS did not converge in any trial, the LS converged for 96% of the trials, with an average time of 196.15 s, the SA converged for 62% of the trials, with an average time of 136.98 s, the GA converged for 58% of the trials, with an average time of 754.66 s, the PSO converged for just 10% of the trials, with an average time of 351.12 s, and the SCBGA converged for 99% of the trials, with an average time of 90.61 s.

Fig. 15 shows boxplot graphics for the number of objective function evaluations for the six algorithms considered and both damping ranges, until the solution was found.

Based on the results shown in Table 2 and Fig. 15, it can be concluded that the SCBGA presents a better performance than all the other algorithms, achieving a solution for the problem with a lower number of objective function evaluations and therefore a lower computational time, for both damping ranges.

For the case with $\xi_{i_{\min}}^{des_1} \geq 10\%$, Table 2 indicates that all the algorithms – except the RS – presented an excellent rate of convergence (more than or equal to 99%). In addition, the maximum and average times of convergence of the SCBGA were lower than the other algorithms considered. The minimum times of convergence were approximately the same for all the methods – except the RS. For the case with $\xi_{i_{\min}}^{des_2} \geq 15\%$, the SCBGA and the LS presented the

Table 2
Comparison the algorithms' performance.

Algorithm	Damping ratio (%)	Number of solutions found for each 10 tests										Time of convergence (s)		
												Average	Min.	Max.
RS	≥10	–	2	2	2	1	1	1	1	1	–	212.72	23.57	420.53
	≥15	–	–	–	–	–	–	–	–	–	–	–	–	–
LS	≥10	10	10	10	10	10	10	10	10	10	10	34.60	1.26	109.55
	≥15	10	10	9	10	10	9	9	10	10	9	196.15	32.59	528.03
SA	≥10	10	10	10	10	10	10	10	10	10	10	89.55	1.94	154.98
	≥15	3	4	9	6	4	7	7	7	9	6	136.98	85.31	316.43
GA	≥10	10	10	10	10	10	10	10	10	10	10	60.90	1.30	203.85
	≥15	4	6	5	7	6	6	6	4	7	7	754.66	234.83	1056.80
PSO	≥10	10	10	10	10	10	10	10	9	10	10	34.34	1.50	203.30
	≥15	1	1	1	1	1	0	2	1	1	1	351.12	148.92	805.09
SCBGA	≥10	10	10	10	10	10	10	10	10	10	10	14.53	1.67	33.71
	≥15	10	10	10	10	10	9	10	10	10	10	90.61	43.78	222.49

better convergence rates, of 99% and 96%, respectively. However, the SCBGA presented a better performance than the LS when the computational times were compared: the SCBGA was 216% faster than the LS on average.

Fig. 15 indicates that for $\xi_{i_{\min}}^{des_1} \geq 10\%$, considering the first and third quartiles of the number of objective functions evaluations, the SCBGA solved the problem with approximately 40–80 evaluations. For this same problem, the GA, PSO, LS, and SA spent more objective function evaluations than the SCBGA. For $\xi_{i_{\min}}^{des_2} \geq 15\%$, considering the first and third quartiles of the number of objective functions evaluations, the SCBGA solved the problem with approximately 200–400 evaluations; much more efficiently than the GA, PSO, LS, and SA. Finally, the results indicate that the RS algorithm is not able to solve this problem adequately.

6.3. Analysis of the stability considering the SCBGA

Based on the data presented in Table 2 and Fig. 15, it can be concluded that the performance of the SCBGA is superior for adjusting the parameters of the PI, PSS, and IPFC-POD controllers to insert

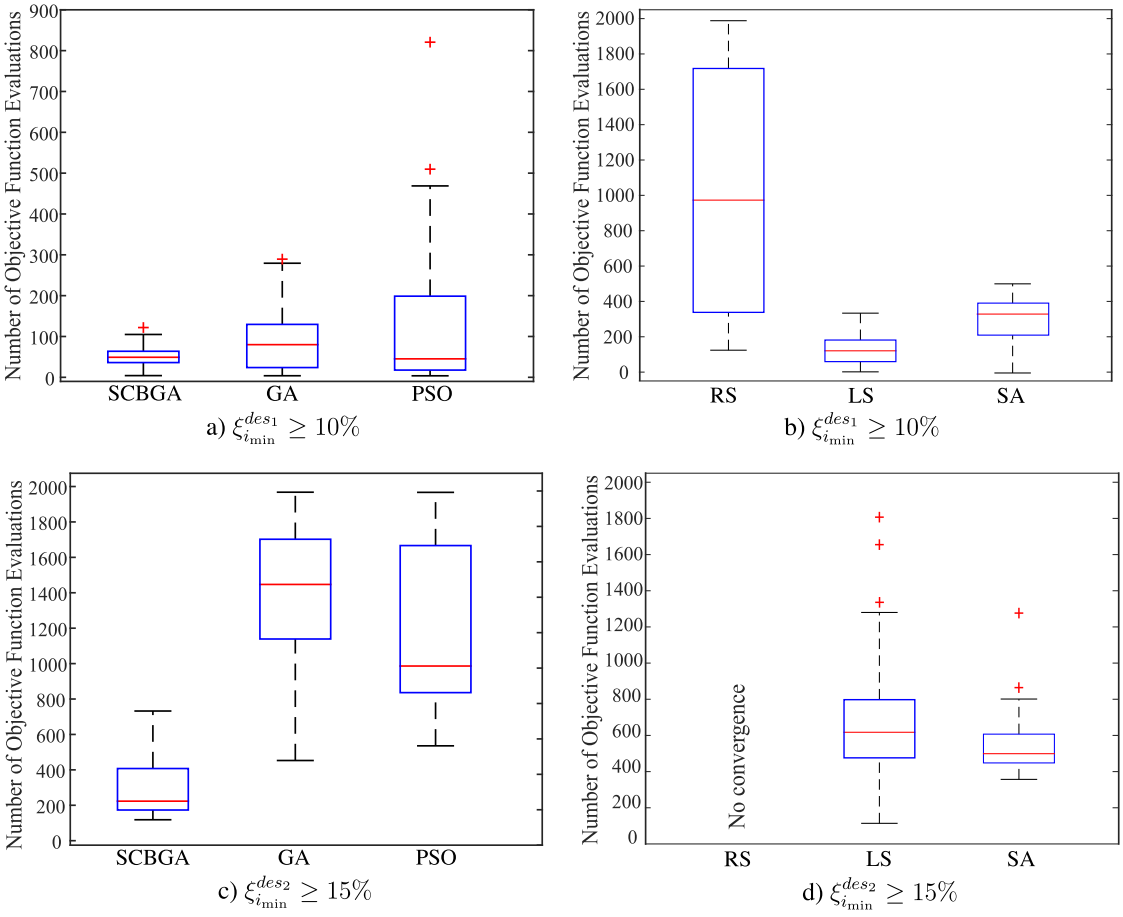

Fig. 15. Number of evaluations of the objective function for the six algorithms, considering $\xi_{i_{\min}}^{des_1} \geq 10\%$ and $\xi_{i_{\min}}^{des_2} \geq 15\%$.

Table 3
Gains (in p.u.) and time constants (in seconds) of the PSS controllers tuned using the SCBGA.

Parameters	PSS *G*1	PSS *G*2	PSS *G*3	PSS *G*4	PSS *G*5	PSS *G*7	PSS *G*8	PSS *G*9
$T_1 = T_3$	1.1000	0.6532	0.6916	0.5940	0.5218	0.3520	0.7314	0.3464
$T_2 = T_4$	0.0617	0.0682	0.0629	0.0715	0.0769	0.0751	0.0362	0.0983
K_{pss}	10.000	6.2716	5.6000	5.5000	6.1367	3.4820	7.5000	6.2951

Table 4
Gains (in p.u.) and time constants (in seconds) of the PI and IPFC-POD controllers tuned using the SCBGA.

IPFC-POD parameters			PIs parameters					
$T_{p_1} = T_{p_3}$	$T_{p_2} = T_{p_4}$	K_{pod}	T_{1_i}	T_{2_i}	T_{3_i}	$K1$	$K2$	$K3$
0.3865	0.2616	0.4000	0.0090	0.0062	0.0065	0.3452	0.6373	1.0068

additional damping to the oscillations of the EPS. Thus, the result of one of the tests performed by SCBGA, considering $\xi_{i_{\min}}^{des_2} \geq 15\%$, is randomly selected and shown in Tables 3 and 4.

The eigenvalues were calculated again for the New England system, considering the effect of the controllers after their parameters were tuned using the SCBGA. The oscillation modes of interest are listed in Table 5.

On analyzing the eigenvalues of Table 5, it is concluded that the controllers made the test system stable at this operating point. Furthermore, the design constraint (minimum damping coefficient of 15% for all oscillation modes of interest) was satisfied. This shows the efficiency of the proposed algorithm (SCBGA) in the tuning of the parameters of the controllers to solve problems related to small signal stability.

Table 5
Dominant eigenvalues (λ_i), damping coefficients (ξ_i), and frequencies (ω_{ni}) considering the effect of the controllers.

Mode	Eigenvalues	ξ_i (p.u.)	ω_{ni} (Hz)
λ_1	$-1.0435 \pm j6.8556$	0.1505	1.1037
λ_2	$-1.3263 \pm j7.1624$	0.1821	1.1593
λ_3	$-1.1342 \pm j6.8101$	0.1643	1.0988
λ_4	$-1.3016 \pm j8.0157$	0.1603	1.2925
λ_5	$-0.7675 \pm j4.6343$	0.1634	0.7476
λ_6	$-1.3635 \pm j7.5024$	0.1788	1.2136
λ_7	$-1.0377 \pm j6.6031$	0.1552	1.0638
λ_8	$-1.1806 \pm j5.8805$	0.1968	0.9546
λ_9	$-0.6459 \pm j4.1381$	0.1542	0.6666

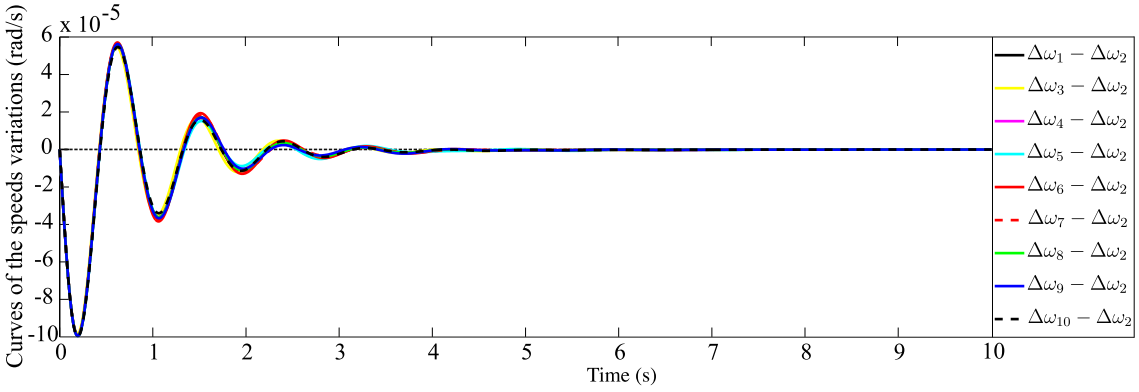

Fig. 16. Variations in the angular speeds of the rotors of the machines of the New England system.

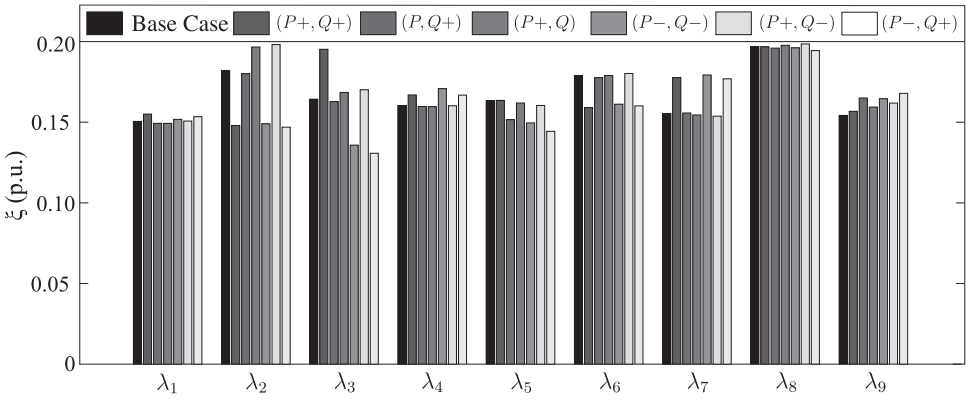

Fig. 17. Comparison of the levels of damping with varying bus loads.

Electrical power systems are constantly subject to small variations of load, and thus consequent generation adjustments. Fig. 16 shows the changes in the angular speeds of the rotors of all generating units of the New England system in relation to the variations in angular velocity of the rotor of the second generator (G2), the system reference generator, when a 0.05 p.u. step in its mechanical power is applied.

The disturbance in the mechanical power of Generator 2 is similar to a small adjustment in the generation that can be caused by a small increase in the system load. Even after the disturbance, the system is well-damped as seen in Fig. 16, which shows graphically the high margin of stability to small perturbations provided by this solution.

The following cases were considered to check the behavior of the New England test system for possible load changes:

- Base case: operating point related to the conditions of the eigenvalues in Table 5;
- Case (P+, Q+): an increase of 5% in both the active and reactive loads;
- Case (P, Q+): the active loads remain unaltered and an increase of 5% in the reactive loads is simulated;
- Case (P+, Q): a 5% increase is applied to the active loads and the reactive loads remain unchanged;
- Case (P−, Q−): a decrease of 5% in both active and reactive loads;
- Case (P+, Q−): an increase of 5% in the active loads and a decrease of 5% in the reactive loads;
- Case (P−, Q+): a decrease of 5% in the active loads and an increase 5% in the reactive loads;

The changes in the loads of the New England system were not defined in the SCBGA algorithm when the tuning of the parameters was performed; thus, damping levels below those specified by the design ($\xi_i^{des} \leq 15\%$) are expected with the variations in loads.

The damping coefficients of oscillation modes after the changes in loads at PQ buses are shown in Fig. 17.

On analyzing Fig. 17, it is possible to conclude that the damping of some oscillation modes of interest remained almost unchanged (λ_1, λ_8, and λ_9), in some cases the damping increased and in others it decreased. Thus in general, the New England system operated with a high level of damping in all the cases analyzed, showing the robustness of the solution obtained by the SCBGA.

7. Conclusions

This work presented a Specialized Chu–Beasley's Genetic Algorithm (SCBGA) to perform coordinated tuning of the parameters of proportional-integral controllers and supplementary damping controllers (power system stabilizers and interline power flow controller-power oscillation damping controller). The objective was to insert additional damping to low frequency electromechanical oscillations of multi-machine electric power systems. The electric power system and the devices were modeled using the current sensitivity model and a new model for the interline power flow controller by current injection was presented.

A static analysis using the New England test system demonstrated the validity of the model for the interline power flow controller. The efficiency of the proposed SCBGA algorithm for tuning of the parameters of the controllers was then analyzed, considering two different damping ranges. The performance (time and number of objective function evaluations to obtain the solution) of the SCBGA was compared with five other optimization methods: a Random Search, a Local Search, a Simulated Annealing, a Genetic Algorithm, and a Particle Swarm Optimization method.

The results for the SCBGA showed that the proposed technique presented a better performance than the other algorithms. In addition, when there were load variations, the solutions obtained with the SCBGA ensured that the system remained stable with a high damping margin, showing the robustness of the solutions obtained by the SCBGA.

Acknowledgments

This work was supported by the Brazilian Federal Agency for the Support and Evaluation of Graduate Education (CAPES), National Council for Scientific and Technological Development (CNPq), under grant 141084/2016-2, and São Paulo Research Foundation (FAPESP), under grant 2014/23741-9.

Appendix A. Data of the New England system

Complete data for the New England system is provided in Tables A.6 and A.7 [18]. In Table A.6, x'_d is the transitory reactance of direct axis, x_d the synchronous reactance of direct axis, x_q the synchronous reactance of quadrature axis, H the inertia constant of the synchronous machine, D the damping torque coefficient of the electromechanical loop, T'_{d_0} the transient direct-axis open-circuit time constant, K_r the gain of the AVR, and T_r the time constant of the AVR. These parameters were used in the CSM [28]. In Table A.7, r is the resistance of the line, x the reactance of the line, b the shunt susceptance of the line, P_g is the active power generation at the end bus of the line, Q_g the reactive power generation at the end bus of the line, P_l the active power demand of the load at the end bus of the line, and Q_l the reactive power demand of the load at the end bus of the line. Bus 2 was the reference bus.

Table A.6
Synchronous generators and excitation system data for the New England system.

Generator	Synchronous generators						Excitation system	
	x'_d (p.u.)	x_d (p.u.)	x_q (p.u.)	H (s)	D (p.u.)	T'_{d_0} (s)	K_r	T_r
1	0.0310	0.1000	0.0609	42.00	4.00	10.20	5.00	0.06
2	0.0697	0.2950	0.2820	30.30	9.75	6.56	6.20	0.05
3	0.0531	0.2495	0.2370	35.80	10.00	5.70	5.00	0.06
4	0.0436	0.2620	0.2580	28.60	10.00	6.56	5.00	0.06
5	0.1320	0.6700	0.6200	26.00	3.00	5.40	40.00	0.02
6	0.0500	0.2540	0.2410	34.80	10.00	7.30	5.00	0.02
7	0.0490	0.2950	0.2920	26.40	8.00	5.66	40.00	0.02
8	0.0570	0.2900	0.2800	24.30	9.00	6.70	5.00	0.02
9	0.0570	0.2106	0.2050	34.50	14.00	4.79	40.00	0.02
10	0.0001	1e−10	1e−10	1e9	10.00	7.00	0.001	9999

Table A.7
Lines and buses data for the New England system.

Initial bus	End bus	r (p.u.)	x (p.u.)	b (p.u.)	P_g (MW)	Q_g (MVAr)	P_l (MW)	Q_l (MVAr)
31	1	0.0000	0.0181	0.0000	250.00	72.97	0.00	0.00
35	**2**	0.0000	0.0250	0.0000	665.82	211.98	9.00	5.00
39	3	0.0000	0.0200	0.0000	650.00	175.91	0.00	0.00
19	4	0.0007	0.0142	0.0000	632.00	132.73	0.00	0.00
20	5	0.0009	0.0180	0.0000	508.00	128.92	0.00	0.00
22	6	0.0000	0.0143	0.0000	650.00	184.49	0.00	0.00
23	7	0.0005	0.0272	0.0000	560.00	127.42	0.00	0.00
25	8	0.0006	0.0232	0.0000	540.00	32.98	0.00	0.00
29	9	0.0008	0.0156	0.0000	830.00	62.95	0.00	0.00
38	10	0.0010	0.0250	1.2000	1000.00	178.39	1214.40	250.00
35	11	0.0007	0.0082	0.1389	0.00	0.00	0.00	0.00
13	12	0.0016	0.0435	0.0000	0.00	0.00	8.00	88.00
39	13	0.0004	0.0043	0.0729	0.00	0.00	0.00	0.00
33	14	0.0008	0.0129	0.1382	0.00	0.00	0.00	0.00
14	15	0.0018	0.0217	0.3660	0.00	0.00	320.00	153.00
15	16	0.0009	0.0094	0.1710	0.00	0.00	329.00	32.00
16	17	0.0007	0.0089	0.1342	0.00	0.00	0.00	0.00
32	18	0.0011	0.0133	0.2138	0.00	0.00	158.00	30.00
16	19	0.0016	0.0195	0.3040	0.00	0.00	0.00	0.00
19	20	0.0007	0.0138	0.0000	0.00	0.00	628.00	103.00
16	21	0.0008	0.0135	0.2548	0.00	0.00	274.00	115.00
21	22	0.0008	0.0140	0.2565	0.00	0.00	0.00	0.00
22	23	0.0006	0.0096	0.1846	0.00	0.00	275.00	85.00
23	24	0.0022	0.0350	0.3610	0.00	0.00	309.00	−92.00
31	25	0.0070	0.0086	0.1406	0.00	0.00	224.00	48.00
25	26	0.0032	0.0323	0.5130	0.00	0.00	139.00	17.00
26	27	0.0014	0.0147	0.2396	0.00	0.00	281.00	76.00
26	28	0.0043	0.0474	0.7802	0.00	0.00	206.00	28.00
26	29	0.0057	0.0625	1.0290	0.00	0.00	284.00	27.00
10	30	0.0010	0.0250	0.7500	0.00	0.00	0.00	0.00
30	31	0.0035	0.0411	0.6987	0.00	0.00	0.00	0.00
31	32	0.0013	0.0151	0.2572	0.00	0.00	322.00	2.00
32	33	0.0013	0.0213	0.2214	0.00	0.00	500.00	184.00
33	34	0.0008	0.0128	0.1342	0.00	0.00	0.00	0.00
34	35	0.0002	0.0026	0.0434	0.00	0.00	0.00	0.00
35	36	0.0006	0.0092	0.1130	0.00	0.00	233.00	84.00
34	37	0.0008	0.0112	0.1476	0.00	0.00	522.00	176.00
37	38	0.0023	0.0363	0.3804	0.00	0.00	0.00	0.00
11	39	0.0004	0.0043	0.0729	0.00	0.00	0.00	0.00
36	37	0.0004	0.0046	0.0780				
13	14	0.0009	0.0101	0.1723				
16	24	0.0003	0.0059	0.0680				
17	18	0.0007	0.0082	0.1319				
17	27	0.0013	0.0173	0.3216				
28	29	0.0014	0.0151	0.2490				
12	11	0.0016	0.0435	0.0000				

References

[1] P. Anderson, A.A. Fouad, Power System Control and Stability, Wiley-IEEE Press, New York, 1993.
[2] F.P. De Mello, C. Concordia, Concepts of synchronous machine stability as affected by excitation control, IEEE Trans. Power Appar. Syst. 88 (4) (1969) 316–329.
[3] E. Larsen, D. Swann, Applying power system stabilizers. Part II: Performance objectives and tuning concepts, IEEE Trans. Power Appar. Syst. PAS 100 (6) (1981) 3025–3033.
[4] R.F. Moura, M.A. Furini, P.B. Araujo, Estudo das limitações impostas ao amortecimento de oscilações eletromecânicas pelos zeros da FTMA de controladores suplementares, Control Autom. 23 (2012) 190–201.
[5] N.G. Hingorani, L. Gyugyi, Understanding FACTS: Concepts and Technology of Flexible AC Transmission System, IEEE, New York, 1999.
[6] M. Noroozian, G. Andersson, Damping of power system oscillations by use of controllable components, IEEE Trans. Power Deliv. 9 (4) (1994) 2046–2054.
[7] M.M. Menezes, P. Araujo, E.V. Fortes, Bacterial foraging optimization algorithm used to adjust the parameters of power system stabilizers and thyristor controlled series capacitor-power oscillation damping controller, in: 2014 11th IEEE/IAS International Conference on Industry Applications (INDUSCON), 2014, pp. 1–6.
[8] D. Valle, P. Araujo, The influence of GUPFC FACTS device on small signal stability of the electrical power systems, Int. J. Electr. Power Energy Syst. 65 (2015) 299–306.
[9] L. Gyugyi, K. Sen, C.D. Schauderr, The interline power flow controller concept: a new approach to power flow management in transmission systems, IEEE Trans. Power Deliv. 14 (3) (1999) 1115–1123.
[10] X.-P. Zhang, Modelling of the interline power flow controller and the generalised unified power flow controller in Newton power flow, IEE Proc. Gener. Transm. Distrib. 150 (3) (2003) 268–274.
[11] D.B. Valle, I. Kopcak, V.F. Da Costa, Modelagem do interline power flow controller (IPFC) no fluxo de carga e análise de carregamento do sistema, in: III Simpósio Brasileiro de Sistemas Elétricos, Belém-Pará, 2010, pp. 1–6, CD-ROM.
[12] S.M. Deckmann, V.F. Da Costa, A power sensitivity model for electromechanical oscillation studies, IEEE Trans. Power Syst. 9 (2) (1994) 965–971.
[13] D. Valle, P. Araujo, Comparação das estruturas de controle do IPFC e de técnicas de ajuste dos parâmetros do controlador POD, in: X Conferência Brasileira sobre Qualidade de Energia Elétrica CBQEE 2013, Araxá – MG, 2013, pp. 1–6.
[14] A. Vinkovic, R. Mihalic, A current-based model of an IPFC for Newton–Raphson power flow, Electr. Power Syst. Res. 79 (8) (2009) 1247–1254.
[15] J. Zhang, A. Yokoyama, T. Ide, Use of IPFC detailed dynamic model for analysis of power flow control and small-signal stability enhancement, IEEJ Trans. Electr. Electron. Eng. 4 (5) (2009) 654–662.
[16] N. Yang, Q. Liu, J.D. McClley, TCSC controller design for damping interarea oscillations, IEEE Trans. Power Syst. 13 (14) (1998) 1304–1310.
[17] G.N. Zhenenko, H. Farah, Simultaneous optimization of the adjustable parameters in multimachine power systems, Electr. Power Syst. Res. 7 (2) (1984) 103–108.
[18] P.B. Araujo, L.C. Zaneta, Pole placement method using the system matrix transfer function and sparsity, Int. J. Electr. Power Syst. Energy Syst. 23 (3) (2001) 173–178.
[19] S. Abd-Elazim, E. Ali, Coordinated design of PSSs and SVC via bacteria foraging optimization algorithm in a multimachine power system, Int. J. Electr. Power Energy Syst. 41 (1) (2012) 44–53.

[20] H. Hasanvand, M.R. Arvan, B. Mozafari, T. Amraee, Coordinated design of PSS and TCSC to mitigate interarea oscillations, Int. J. Electr. Power Energy Syst. 78 (2016) 194–206.
[21] H. Shayeghi, A. Safari, H.A. Shayanfar, PSS and TCSC damping controller coordinated design using PSO in multi-machine power system, Energy Convers. Manage. 51 (12) (2010) 2930–2937.
[22] L.H. Hassan, M. Moghavvemi, H.A.F. Almurib, K.M. Muttaqi, A coordinated design of PSSs and UPFC-based stabilizer using genetic algorithm, IEEE Trans. Ind. Appl. 50 (5) (2014) 2957–2966.
[23] J.H. Holland, Adaptation in Natural and Artificial Systems: An Introductory Analysis with Applications to Biology, Control, and Artificial Intelligence, Bradford Book, MIT Press, 1992.
[24] P. Chu, J. Beasley, A genetic algorithm for the generalised assignment problem, Comput. Oper. Res. 24 (1) (1997) 17–23.
[25] F. Glover, G. Kochenberger, Handbook of Metaheuristics International Series in Operations Research & Management Science, vol. 57, Springer, US, 2003.
[26] J. Kennedy, R. Eberhart, Particle swarm optimization, in: IEEE International Conference on Neural Networks, vol. 4, 1995, pp. 1942–1948.
[27] K. Michalewicz, Genetic algorithms + data structures = evolution programs, 2nd ed., Springer, Berlin, 1994.
[28] C.R. Pádua Júnior, A.L.M. Takahashi, M.A. Furini, P. Araujo, Proposta de um modelo para análise de estabilidade a pequenas perturbações baseado na lei de Kirchhoff para correntes, in: SBAI/DINCON 2013, Fortaleza – CE, vol. 3, 2013, pp. 1–6.
[29] J. Zhang, A. Yokoyama, Power system transient stability improvement by the interline power flow controller (IPFC), IEEJ Trans. Power Energy 128 (1) (2008) 208–215.
[30] N. Rezaei, M. Kalantar, H.A. Shayanfar, Y. Alipouri, A. Safari, Optimal IPFC signal selection and damping controller design using a novel current injection model in a multi-machine power system, Int. J. Electr. Power Energy Syst. 44 (1) (2013) 461–470.
[31] P. Kundur, Power System Stability and Control, MacGraw-Hill, New York, 1994.